Inverse Problems **24** (2008) 065010 (17pp) doi:10.1088/0266-5611/24/6/065010

Computed myography: three-dimensional reconstruction of motor functions from surface EMG data

Kees van den Doel, Uri M Ascher and Dinesh K Pai[1]

Department of Computer Science, University of British Columbia, Canada

Received 10 June 2008, in final form 30 September 2008
Published 6 November 2008
Online at stacks.iop.org/IP/24/065010

Abstract

We describe a methodology called computed myography to qualitatively and quantitatively determine the activation level of individual muscles by voltage measurements from an array of voltage sensors on the skin surface. A finite element model for electrostatics simulation is constructed from morphometric data. For the inverse problem, we utilize a generalized Tikhonov regularization. This imposes smoothness on the reconstructed sources inside the muscles and suppresses sources outside the muscles using a penalty term. Results from experiments with simulated and human data are presented for activation reconstructions of three muscles in the upper arm (biceps brachii, bracialis and triceps). This approach potentially offers a new clinical tool to sensitively assess muscle function in patients suffering from neurological disorders (e.g., spinal cord injury), and could more accurately guide advances in the evaluation of specific rehabilitation training regimens.

(Some figures in this article are in colour only in the electronic version)

1. Introduction

The aim of the methods described in this paper is to provide a detailed mapping of the activity of individual muscles by using surface electromyography (sEMG) data from multiple recording sites. We call the resulting system computed myography (CMG).

Muscle activity monitoring can be used for the diagnosis of musculoskeletal deficits, such as those arising from spinal cord injury or stroke, and for guiding rehabilitation. Conventional monitoring of a patient recovery process is restricted to describing a general pattern of recovery [3], mostly based on functional assessments. The CMG system proposed in this paper has the potential to display detailed activity changes in individual muscles. Basic research in motor control, for instance aimed at measuring muscle synergies [1], would also benefit from a tool to measure individual muscle activities. See, e.g., [3, 5, 6, 10, 25] for further clinical detail.

[1] This work was supported in part by the Peter Wall Institute for Advanced Studies, Canada Research Chairs Program, NSERC, CFI and BC KDF.

The novelty of the present work is in the application of inverse problem techniques. Moreover, to produce an effective tool for medical diagnostics and to compare synthetic experiments against those for human measured data, a detailed 3D modeling of the spatial domain (which is that of a limb) must be performed.

The sources of electrical signals originating from muscle fibers are relatively well understood; both simple and detailed forward models for these are available, see [27]. For example, in [24] a multi-layer finite element method (FEM) model of an idealized cylindrical limb was used to predict the sEMG signal detected when a single source is present.

The inverse problem is to reconstruct current sources, inside muscles of a limb, using simultaneous spatial information from a surface-mounted grid of sEMG sensors. The reconstructed sources are such that the measured sEMG data are subsequently explained by the model. This inverse problem, in its general form, is well known [18] to have no unique solution, i.e. many different sources can fit the data exactly. We must, therefore, constrain the solution to the inverse problem appropriately.

A simple-minded approach is to select the solution with minimum norm [17]. However, because signals from deep sources decay when propagating to the surface due to volume conduction, they need to be stronger than superficial sources to explain the data. This method would, therefore, place the reconstructed sources as close as possible to the sensors, and is thus unable to detect deep sources. A more promising approach incorporates *a priori* information into the regularization process by imposing some measure of solution smoothness. This can be done by weighting the minimum least-squares norm of the solution with that of its gradient, thus introducing the Laplacian operator under the necessary conditions [28, 29]. The physiological basis for this well-known approach is that activity in nearby regions is correlated within muscles. Note though that this yields blurred reconstructions. The amount of blurring decreases when the number of surface data is increased up to an upper limit, when the maximum resolution has been obtained. In many of our applications, we are only interested in the integrated activity over a specific muscle region, and in this case the details which are lost due to blurring are probably not important.

1.1. Related work

The only previous work [2, 19, 23, 31] on source localization in sEMG that we are aware of uses an overdetermined discrete source model (see below for details on this type of models). These efforts seem to be of a preliminary nature.

Clinical applications of high density sEMG were reviewed in [9]. These applications focus mainly on measuring detailed properties such as the pulse shape of individual motor unit (MU) action potentials and utilizing multiple surface electrodes as an alternative to needle EMG. They do not focus on a comprehensive mapping of the current sources within a muscle (i.e. localization). The corresponding methods require similar measurement techniques as our proposed method, i.e. utilizing a grid of simultaneous sensors, whereas the data analysis part has no overlap with our method. See, for example, the HD-sEMG hardware described in [22].

Temporal information can be used to attempt to separate the mixing of signals from multiple motor units ('crosstalk') in the sEMG signals. With advanced processing methods such as 'precision decomposition' [4], it is possible to separate up to five MUs. In many applications, crosstalk elimination (or reduction) is a central challenge; see, for example, [4, 20]. While this is not our main goal and so will not be further pursued here, we note that our approach can also achieve a level of crosstalk reduction. If we reconstruct the current sources within the individual muscles, it is then possible to calculate what the sEMG signal

would be if only a particular muscle of interest was active. Thus, we eliminate the signals from the other co-activated muscles.

However, for our purposes crosstalk is not a problem but rather part of the solution, as it is precisely the mixing of signals from different locations in individual voltage sensors that enables the reconstruction of spatial information of the various current sources in the muscles.

Activity source localization within the brain from surface electroencephalogram (EEG) data has been an active area of research for decades, and it has close connections to our proposed methodology. A recent review of the state of the art of EEG inverse modeling can be found in [28]. The sEMG inverse problem has many similarities to the EEG inverse problem, and we will therefore review some of this material on EEG source localization and highlight the relations to the inverse sEMG problem. In a typical clinical practice, the number of monopolar EEG electrodes conventionally used is about 20, but localization can be improved by increasing this number up to 60, whereas increases in recording electrode numbers have only a marginal effect in sensitivity or accuracy [28]. It is also important to sample the scalp uniformly with the available electrodes. Two distinct EEG inverse modeling approaches are used to localize sources in the brain [28]. The first goes under the name 'overdetermined discrete source models'. In this approach, the sources are assumed to be a small number of current dipoles and they are placed to best fit the data, as predicted by a forward model (i.e. a model that can predict measured surface EEG data from a model of the current sources in the brain). The number of sources is taken such that the number of unknown parameters is less than the number of independent measurements (i.e. data at the electrodes) so that the solution is unique. The intrinsic problem with this method is that the number of dipole sources cannot be determined in advance, and that only a limited number of sources can be reconstructed, whereas cortical activity can involve a large number of sources. Therefore, models that make no prior assumption about the number of sources have received increased attention. Since the number of electrical sources in a normally active muscle is also large, we believe that this method is not well suited to the reconstruction of muscle activation patterns.

The second method is referred to as 'underdetermined distributed source models'. In this approach, the domain is subdivided into a large number of voxels and a distinct dipole current source value (an activation) is assigned to each voxel. The task is then to find a configuration of values in the voxels that explain the data. Because a large number of voxels are used, this problem is underdetermined, i.e. many patterns of activation can fit the measurements exactly or up to the noise level. Regularization is necessary to make the solution stable and locally unique so that small variations in the data do not cause large variations in the solution. Various different weighting strategies that do not penalize deep sources heavily have been proposed [11, 13, 14, 16]. However, there is no physiological basis for these weighting strategies. A more promising method penalizes lack of solution smoothness, as explained earlier [28, 29]. The physiological basis for this approach is that neural activity in nearby regions is correlated. Since the same is true in muscles, we believe that this approach, appropriately modified for sEMG, is the most promising one for our purpose.

In section 2, we proceed to develop our method, discussing both modeling and computational issues. In section 3, we then put the method to the test and report on results from four experiments involving synthetic as well as human data. Conclusions are offered in section 4.

2. Forward and inverse modeling

We wish to reconstruct muscle activations through sEMG, that is, from measurements of the electric potential on the surface (skin). The sources of the potential field are polarization

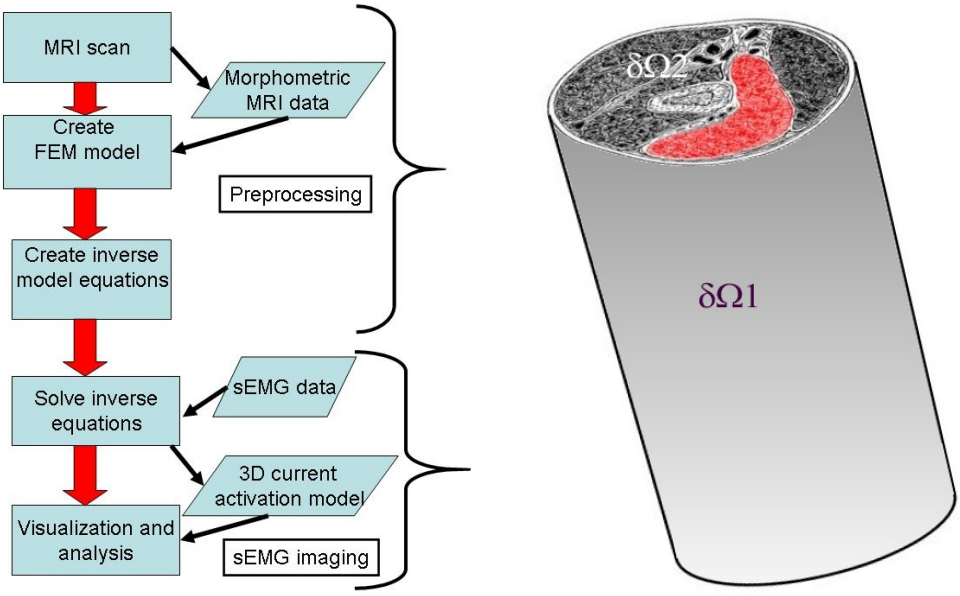

(a) Systems diagram (b) 3D geometry

Figure 1. (a) Diagram of the CMG system. The thick arrows indicate sequential processing steps, the thin arrows indicate data produced or used, rectangles represent processes and the slanted rectangles represent data. The preprocessing is done once for a patient and remains valid as long as no significant change in morphology takes place. (b) A 3D domain Ω (consisting of muscle, fat and bone) with the physical boundary $\partial\Omega_1$ (gray) and the cut boundary (textured) $\partial\Omega_2$.

waves called 'intracellular action potentials' (IAP) which travel outward over the individual muscle fibers starting at the axon connection, roughly in the middle of the muscle fiber. Each MU is a collection of muscle fibers which is excited more or less synchronously. Typically, there are 100–1000 MUs per muscle which may or may not be temporally dependent. The speed of the action potential traveling over the fiber (about 3–5 m s^{-1}) is called the conduction velocity. It is proportional to the radius of the fiber. The 'motor unit action potential' (MUAP) is the resultant depolarization wave of all the fibers in a particular MU. The wave shape of the IAP is known, and standard models exist to describe it. The length of the pulse is typically 2–40 mm. The most primitive model is a *tripole* traveling outward in pairs; more sophisticated models use parameterized functions. The speed of the action potentials is sufficiently slow so that electrical potential propagation can be considered instantaneous. Usually, sEMG data in the frequency domain are considered up to 500 Hz (2000 Hz for needle EMG).

2.1. Methodology

Our source localization methodology consists of the following steps, illustrated in figure 1.

(i) Acquire a three-dimensional geometry model by the segmentation of MRI data.
(ii) Build a forward model for 3D volume conduction which can predict surface voltages (i.e. it can predict the data) from given current sources in the muscles.

The electrostatic potential $u(\mathbf{x})$ satisfies the generalized Poisson partial differential equation (PDE) on the domain Ω

$$-\nabla(\boldsymbol{\sigma}\nabla)u = I(\mathbf{x}) \quad \text{in } \Omega, \tag{1a}$$

$$\nabla_{\boldsymbol{n}} u = 0 \quad \text{on } \partial\Omega_1, \tag{1b}$$

$$\nabla_{\boldsymbol{n}} u = -\Sigma u \quad \text{on } \partial\Omega_2. \tag{1c}$$

Here, $\boldsymbol{n}$ is the outward normal at the boundary and $\boldsymbol{\sigma}(\mathbf{x})$ is the conductivity tensor (note that it is not isotropic in the muscles). The source $I(\mathbf{x})$ is the transmembrane current density, which we assume is proportional to the second spatial derivative along the muscle fiber direction of the muscle fiber intracellular action potential $V(\boldsymbol{x}, t)$. We distinguish two types of boundaries: the physical boundary $\partial\Omega_1$, representing skin on which data can be measured, and the cut boundary $\partial\Omega_2$, which represents the artificial boundary of our model (i.e. a cut through the arm; see figure 1(b)). The Σ term is an effective resistance modeling the flow of currents in and out of our modeling domain at its artificial boundaries.

(iii) Solve the inverse problem by computing the most likely current sources that can explain measured data.

Such an inversion problem is typically ill-posed, which means that the solution is not unique and/or the solution does not continuously depend on the data. Regularization utilizing *a priori* information is then employed to incorporate our prior knowledge of the electrical activities in the muscles. This knowledge includes properties such as smoothness and the regions of possible activation. We then reconstruct the current sources $m(\mathbf{x})$ in the muscle fibers by minimizing the least-squares data fitting error plus a generalized Tikhonov regularization penalty function that incorporates our *a priori* information.

2.2. *Inverse problem formulation*

Denote our measured data, which are (linear combinations of) voltages at specific points on the skin $\partial\Omega_1$, by the vector $\boldsymbol{b}$ with components $b_k, k = 1, \ldots, K$. Define the linear operator $\boldsymbol{Q}$ which produces a vector of corresponding measurements from a potential field $u(\mathbf{x})$. The measurements can be monopolar, differential or any other linear form. Note that $\boldsymbol{Q}$ also carries information about the reference electrode, when used. For example, consider K differential electrodes which measure voltage differences between locations $\boldsymbol{p}_k$ and $\boldsymbol{q}_k$. We have $b_k = u(\boldsymbol{p}_k) - u(\boldsymbol{q}_k)$, and the operator $\boldsymbol{Q}$ can be written as

$$Q(k, \boldsymbol{x}) = \delta^3(\boldsymbol{p}_k - \boldsymbol{x}) - \delta^3(\boldsymbol{q}_k - \boldsymbol{x}),$$

with δ^3 being the three-dimensional Dirac function. The transpose operator $\boldsymbol{Q}^T$ has components $Q^T(\boldsymbol{x}, k) = Q(k, \boldsymbol{x})$. It produces a field $u(\mathbf{x})$ which takes values (in a distribution sense) b_k at $\boldsymbol{p}_k$ and $-b_k$ at $\boldsymbol{q}_k$. For another example, consider monopolar electrodes. Because voltage is only defined up to an additive constant, we need to define a reference voltage. A good choice is the average voltage over all electrodes $\boldsymbol{p}_k$, leading to

$$Q(k, \mathbf{x}) = \delta^3(\boldsymbol{p}_k - \boldsymbol{x}) - \frac{1}{K}\sum_{l=1}^{K} \delta^3(\boldsymbol{p}_l - \boldsymbol{x}).$$

The inverse problem is to find a current density source I that produces a potential field $u(\mathbf{x})$ satisfying (1) such that $\boldsymbol{Q}u(\mathbf{x}) \approx \boldsymbol{b}$. Let us write $I(\mathbf{x}) = \boldsymbol{D}m(\mathbf{x})$, where m is the source function to be reconstructed. The operator $\boldsymbol{D}$ can be taken to be the identity, in which case m is just the current density I, or (without loss of generality) we can choose (assuming that the muscle fibers are aligned in the z-direction) $\boldsymbol{D} = \mathrm{d}^2/\mathrm{d}z^2$, in which case m is the transmembrane potential V. More complicated operators $\boldsymbol{D}$ based on known properties of the

IAP are possible too. Which choice of $\boldsymbol{D}$ will produce the best reconstructions is unclear in general, and we determine the best choice experimentally in the following.

We subdivide the domain Ω explicitly into various regions of interest (ROI) Ω_r such as muscle, fat, bone and skin, each with distinct conductivity properties. The regularized inverse problem is then formulated as the following constrained optimization problem:

$$\min_{m,u}\phi \equiv \frac{1}{2}\|\boldsymbol{Q}u - \boldsymbol{b}\|^2 + \frac{\beta}{2}\sum_r \int_{\Omega_r} (\nabla m \cdot \boldsymbol{W}_r \nabla m + \mu_r m^2)\,\mathrm{d}\mathbf{x}, \tag{2}$$

subject to

$$\begin{aligned} &-\nabla(\sigma_r \nabla)u = \boldsymbol{D}m \quad \text{in } \Omega_r,\\ &\nabla_n u = 0 \quad \text{on } \partial\Omega_1,\\ &\nabla_n u = -\Sigma u \quad \text{on } \partial\Omega_2, \end{aligned}$$

with constant matrices $\boldsymbol{W}_r$ and scalars β and μ_r. We distinguish ROI where we have possible nonzero sources m and other regions such as fat, bone and muscle which we know *a priori* to be inactive. In the ROI, we normalize the matrix $\boldsymbol{W}_r$ to satisfy $\mathrm{trace}(\boldsymbol{W}_r) = 3$. It determines the anisotropy of the smoothing operator which we allow to have different values in the fiber direction and in the orthogonal directions. It is a constant diagonal matrix if the muscle fibers are aligned with one of the coordinate axes. Outside the ROI, we set $\boldsymbol{W} = \boldsymbol{0}$. The damping factors μ_r are taken to be small or zero in the ROI and are set to a large value ($O(1/\beta)$) outside the ROI to suppress reconstruction of sources there. The value of the regularization parameter β balances the relative weights given to the least-squares difference between predicted and measured data versus the *a priori* properties imposed on the solution. Extensive literature (see, for example, [32] for a review) exists on how to determine this parameter.

To write (2) in the Lagrangian form, we introduce the forward operator $\boldsymbol{A}$ corresponding to the forward equations (1) (including boundary conditions), and similarly define the regularization operator $\boldsymbol{Z}$ through

$$\beta\sum_r \int_{\Omega_r} (\nabla m \cdot \boldsymbol{W}_r \nabla m + \mu_r m^2)\,\mathrm{d}\mathbf{x} = \int_\Omega m\boldsymbol{Z}m\,\mathrm{d}\mathbf{x}.$$

Introducing Lagrange multipliers $\lambda(\mathbf{x})$, we obtain the Lagrangian

$$\mathcal{L}(u, m, \lambda) = \frac{1}{2}\|\boldsymbol{Q}u - \boldsymbol{b}\|^2 + \frac{1}{2}\int_\Omega m\boldsymbol{Z}m\,\mathrm{d}\mathbf{x} + \int_\Omega \lambda(\boldsymbol{A}u - \boldsymbol{D}m)\,\mathrm{d}\mathbf{x}, \tag{3}$$

and the resulting system of PDEs forming the necessary conditions for a minimum is

$$\boldsymbol{A}u - \boldsymbol{D}m = 0, \tag{4a}$$

$$\boldsymbol{A}\lambda + \boldsymbol{Q}^T\boldsymbol{Q}u = \boldsymbol{Q}^T\boldsymbol{b}, \tag{4b}$$

$$\boldsymbol{Z}m - \boldsymbol{D}\lambda = 0. \tag{4c}$$

Equations (4) must further be discretized in order to enable an effective numerical simulation. Moreover, an arm cross-section does not have a simple rectangular or spherical geometry, so a finite element method employing a nontrivial mesh must be used. We discretize (4) using the COMSOL Multiphysics Finite Element Modeling software using tetrahedral meshes with second-order isoparametric elements (called 'Lagrange elements' in COMSOL). The resulting sparse indefinite linear system cannot be solved by any of the built-in iterative solvers of COMSOL, but we can extract the coefficients of the linear system and export these to MATLAB. The resulting indefinite system of equations can be reduced in a standard way to

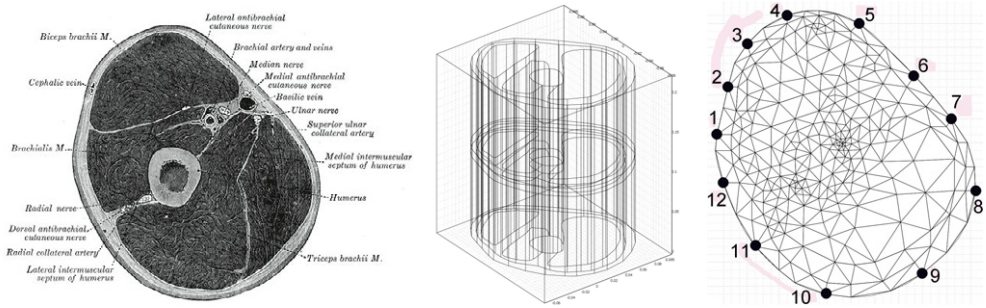

(a) Anatomical image (b) 3D geometry constructed (c) Mesh and 12 sensors

Figure 2. (a) Cross-section of a generic upper arm. The image was segmented into different anatomical regions: brachialis, biceps, triceps, fat and skin, and bone. The resulting 2D regions were then extruded in the vertical direction to create a 3D geometry (b) and imported into the finite element software COMSOL. The 3D geometry was then meshed with tetrahedral elements, and the differential equations were discretized in COMSOL and exported to MATLAB. For the inverse problem so constructed we could then use measured data, or else generate synthetic data, for example at the locations shown in the cross-sectional view of the mesh (c), placing known current sources in the muscles.

a smaller but less sparse positive definite system by eliminating the variables corresponding to u and λ. This leads to

$$(\boldsymbol{D}\boldsymbol{A}^{-1}\boldsymbol{Q}^T\boldsymbol{Q}\boldsymbol{A}^{-1}\boldsymbol{D} + \boldsymbol{Z})\boldsymbol{m} = \boldsymbol{D}\boldsymbol{A}^{-1}\boldsymbol{Q}^T\boldsymbol{b}, \tag{5}$$

where $\boldsymbol{m}$ is a vector of the N degrees of freedom resulting from the discretization of the continuous field $m(\mathbf{x})$. Similarly, the other variables $(\boldsymbol{D}, \boldsymbol{A}, \boldsymbol{Q}, \boldsymbol{Z}, \boldsymbol{b})$ are the matrix representations of the linear operators introduced previously. We solve this linear system of equations numerically using a preconditioned conjugate gradient (PCG) method with the preconditioner $\boldsymbol{Z}^{-1}$. For each PCG iteration we need to compute a product $\boldsymbol{D}\boldsymbol{A}^{-1}\boldsymbol{Q}^T\boldsymbol{Q}\boldsymbol{A}^{-1}\boldsymbol{D}\boldsymbol{v}$ (for some vector $\boldsymbol{v}$), which requires the solution of two forward problems. The latter is accomplished by an inner PCG iteration with an ILU preconditioner. This solution method is similar to that used in [7, 8]. The outer PCG iteration was terminated when the relative residual is less than 10^{-4}.

3. Reconstruction results

3.1. Experimental setup

We have created a 3D geometry of a section of the upper arm, based on the image displayed in figure 2(a), taken from [15]. The image was manually segmented into subcutaneous fat and skin, bone, brachialis, biceps and triceps. We use a lumped model for subcutaneous fat and skin, but intend to extend the model with a boundary layer of skin. The segmented geometry was then imported into COMSOL and we extruded the slice by 20 cm in the vertical direction to create a 3D geometry. Conductivities were assigned to the different regions using the values reported in [24]. The geometry was meshed with tetrahedral elements. A coarse mesh of 32 607 elements was used for the data inversion, whereas a finer mesh of 61 452 elements was used to generate synthetic measurement data, so as to avoid so-called 'inverse crimes'. The system of equations (4) was entered in COMSOL and discretized with an FEM method

using second-order Lagrange elements. The resulting system of discretized partial differential equations was solved outside COMSOL as described above following (5).

The top and bottom of our arm model are modeled as an effective resistance, with the resistance calculated from a 10 cm uniform section of the appropriate material (fat, muscle or bone). For the model to be valid, the artificial boundaries have to be sufficiently distant from the sources so that they have a negligible influence. We have verified explicitly that none of our results depend on the precise value of this effective resistance parameter.

The inversion method was first tested with synthetic simulated data from a single tripole source, then with 5000 randomly placed sources in a single muscle or in a combination of muscles and several configurations of simulated sensors, and finally with data from a human subject. For the tripole model we use the simplest triangular model, with a pulse length of 1cm. No difference in results was observed when the slightly more detailed Rosenfalck model [30] was employed instead. If so desired more realistic models for the IAP (for example, [26, 27]) could be used, but since we use our sources only to test the inversion method there is no need for higher model accuracy here.

3.2. Experiment 1: discriminating brachialis and biceps

The first experiment investigates the ability to discriminate between activations of the biceps and the brachialis. The biceps muscle lies between large portions of the brachialis and the electrode array, and we can therefore expect the brachialis to be less 'visible' to the sensors. In this experiment, the reconstructed sources were constrained to the biceps and brachialis with a large penalty term μ_r in the triceps. We placed 5000 sources in the biceps, in the brachialis or in both. The sources were restricted to the middle 10 cm of the slice in the vertical direction, in order to be sufficiently far from the artificial boundaries. The forward solution Qu was then computed at 215 points on the surface grid, and a 5% random Gaussian noise was added to it. This is referred to below as 'surface data'. The surface data were then restricted to a set of 56 points in a ring around the center ('ring data').

The reconstructions were evaluated with the 3D visualization tools provided by COMSOL as well as by calculating the current source power density in individual muscles, defined as the average of m^2 over a muscle. This is an objective measure of activation of the whole muscle. For the reconstructions, we then measure the *ratio* of biceps and brachialis activations.

Experimentally, we found that the best reconstructions were obtained using $\boldsymbol{D} = 1$, $\mu_r = 0$ in the ROI, $\beta = 10^{-11}$ and $\boldsymbol{W} = \mathbf{1}$. The source m was constrained to attain very small values outside the muscle regions using a penalty method with $\mu_r = 1000/\beta$ outside the ROI. The value of the regularization parameter β was tuned to result in a data discrepancy of about 1.5 times the value derived from the noise level. The results are depicted in figures 3–5. The configuration with surface data gives good reconstructions as judged by visualization or by using the power density metric displayed under the figures. Significantly reduced accuracy is observed with the ring data when only the brachialis is active as the biceps also appears co-activated, though only with half the power density of the brachialis.

3.2.1. Sensitivity analysis. Assessing the sensitivity of the reconstruction to uncertainties in the conductivity parameters (which appear in the forward model (1)) is important, as these are not known very accurately [24]. To determine the effect of these, we have repeated the experiment with sources in the biceps only, as in figure 4, for several modifications of the conductivity parameters. The artificial data are calculated with the same conductivity values as before. But then, the conductivity parameter values are modified in the forward model that is used during the inverse problem reconstruction. Table 1 displays the results. The

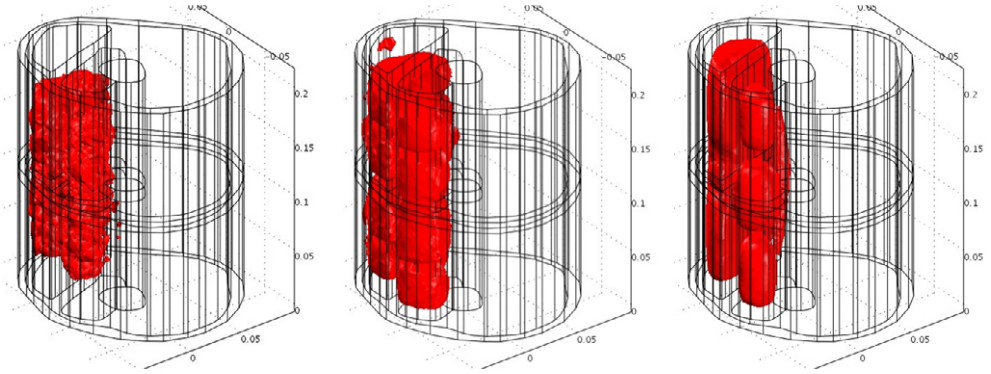

(a) Synthetic source model (b) Reconstructed model with surface data (215 points) (c) Reconstructed model with ring data (56 points)

Figure 3. Experiment 1: (a) 5000 synthetic current tripole sources placed at random locations in the biceps and brachialis. The region of activation is visualized by displaying a surface that encloses 80% of the current sources as measured by the integrated current power. The current sources are then displayed as reconstructed from the surface data (b) and from the more restricted, ring data (c). For the ratio (theoretically = 1) of biceps and brachialis activations, we obtain ratio = 0.953 using the surface grid of 215 data and ratio = 0.91 using the 56 points on a ring.

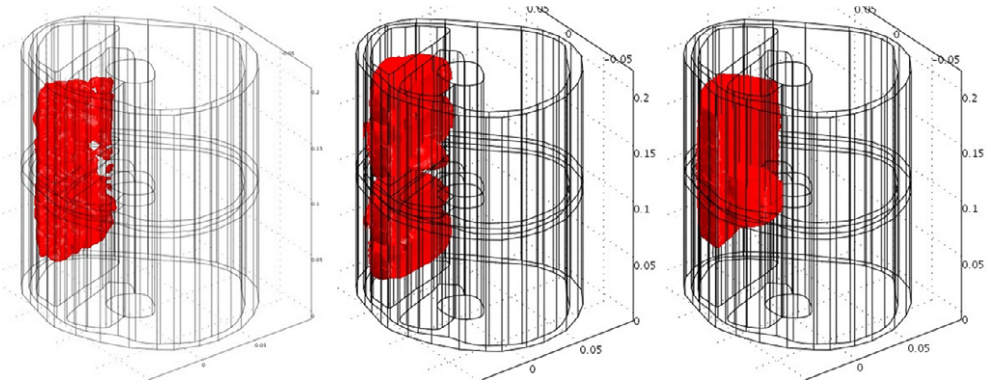

(a) Synthetic source model (b) Reconstructed model with surface data (215 points) (c) Reconstructed model with ring data (56 points)

Figure 4. Results as in figure 3 with artificial sources placed in the biceps only. The reconstructions give for the ratio (theoretically = 0) of brachialis and biceps activations: ratio = 0.03 using the surface grid of 215 data and ratio = 0.05 using the 56 points on a ring.

parameters are multiplied by the values indicated in the table, and the ratio of brachialis and biceps activation is shown for various configurations. The results are rather insensitive to the bone and fat conductivities, whereas the sensitivity to the muscle conductivities is higher. If the transversal or longitudinal conductivity is off by a factor of 2, the error (which is 3% with the correct conductivity values) can become as high as 18%. If the anisotropy ratio is held fixed, i.e. longitudinal and transversal muscle conductivities are both off by the same factor of 2, then the effect is much smaller, leading only to a doubling of the error. We conclude that the anisotropy is the most sensitive parameter in the reconstruction. If this parameter is not known accurately enough, it may be necessary to tune it experimentally by performing the

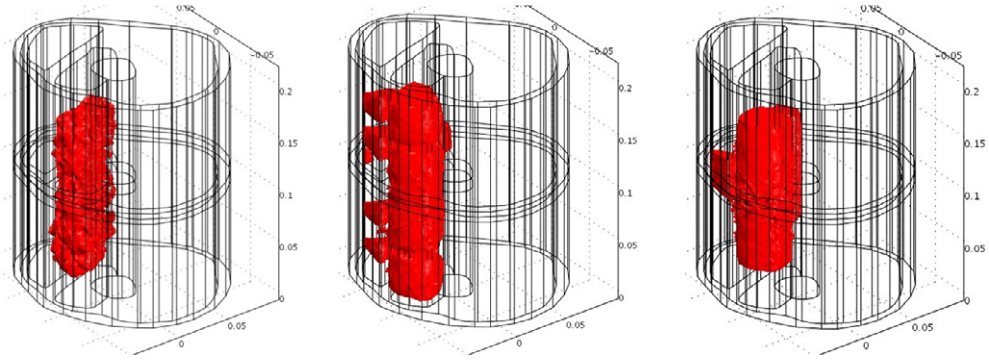

(a) Synthetic source model (b) Reconstructed model with surface data (215 points) (c) Reconstructed model with ring data (56 points)

Figure 5. Results as in figures 3 and 4 with artificial sources placed in the brachialis only. The reconstructions give for the ratio (theoretically = 0) of biceps and brachialis activations: ratio = 0.11 using the surface grid of 215 data and ratio = 0.54 using the 56 points on a ring. In the ring configuration, 35% of the activity is erroneously attributed to the biceps instead of the brachialis, which indicate that this sensor configuration is not adequate. As the brachialis is mostly covered by other muscles, it is the hardest to identify.

Table 1. The conductivities of fat, bone and muscle used for the inverse model in transversal (T) and longitudinal (L) directions are multiplied by the tabulated factors. The ratio of brachialis and biceps activations is used as error measure for the reconstruction.

Fat	Bone	Muscle (T)	Muscle (L)	Error (%)
1	1	1	1	3.0
4	1	1	1	4.0
0.25	1	1	1	3.7
1	4	1	1	2.9
1	0.25	1	1	3.1
1	1	1.5	1	9.0
1	1	0.75	1	3.2
1	1	2	1	15
1	1	0.5	1	14
1	1	1	1.5	7.5
1	1	1	0.75	8.7
1	1	1	2	14
1	1	1	0.5	18
1	1	2	2	6.1
1	1	0.5	0.5	4.2

reconstruction under controlled circumstances (where we know what the result should be) for several values.

In the subsequent experiments, we considered potential sources in all three muscles.

3.3. Experiment 2: single source localization

The ability to localize a single artificial source is sometimes used as a performance measure for source imaging in EEG. In particular, the LORETA [28, 29] method features zero localization error. While we believe that this feature is probably not very relevant for our situation where

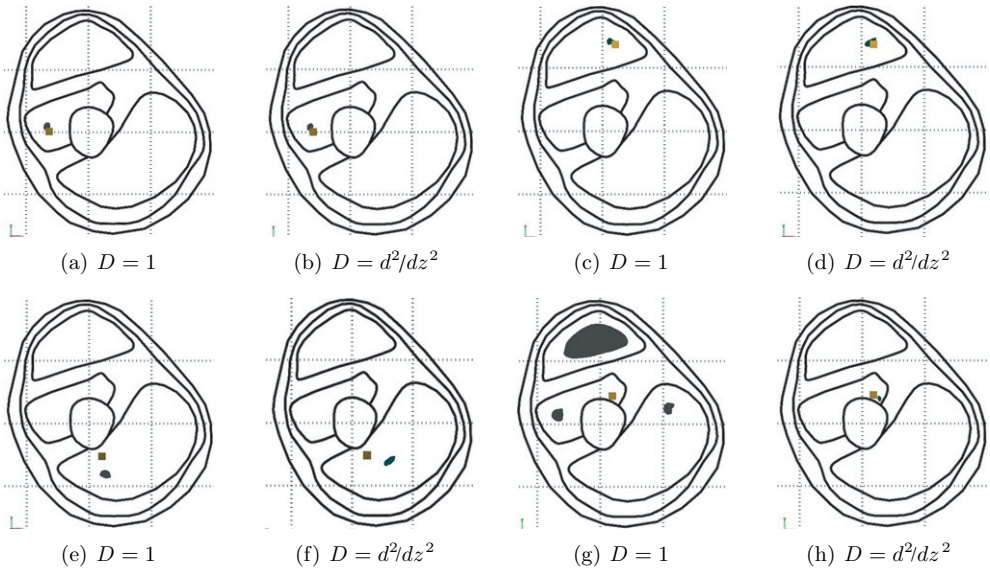

(a) $D = 1$ (b) $D = d^2/dz^2$ (c) $D = 1$ (d) $D = d^2/dz^2$

(e) $D = 1$ (f) $D = d^2/dz^2$ (g) $D = 1$ (h) $D = d^2/dz^2$

Figure 6. Reconstructions of the location on a single tripole source. The true position is indicated by a lighter square and the reconstructed position is indicated by the black shape. In (g) $m(\mathbf{x})$ had multiple local maxima and we indicate the region obtained by thresholding m to show the three maxima.

many thousands of sources are active, we have tested our method by placing a single tripole source at various locations in the three muscles and collecting data on the full surface grid. For $D = 1$ we use the same parameters as before, whereas for $D = \mathrm{d}^2/\mathrm{d}z^2$ we use $\beta = 10^{-6}$. The values of β were chosen to result in a data discrepancy of 1.5 times the value predicted from the known noise level which was again 5%. The reconstructed source locations were then identified with the maximum of $m(\mathbf{x})$. The results are depicted in figure 6. A noticeable localization error occurs in (e) and (f), presumably due to the deep location of the source near the bone. The reconstruction failed in (g) for the deepest source in the brachialis, where three local maxima were found using $D = 1$. However, in this case, the reconstruction with $D = \mathrm{d}^2/\mathrm{d}z^2$ was quite accurate.

3.4. Experiment 3: discriminating brachialis, biceps and triceps

In this experiment, we placed artificial sources in all three muscles in five combinations: sources in a single muscle, equal amount in the brachialis and biceps, and equal amount in all three. Reconstructions were then made, and the source power per muscle (the average value of m^2 on a muscle) was calculated for analysis. We tried both $D = 1$ and $D = d^2/z^2$, and full surface data and ring data (as in experiment 1). While the results of the two choices for D made little difference using full surface data, with $D = 1$ being somewhat better, the reconstruction with data on the ring failed completely for $D = \mathrm{d}^2/\mathrm{d}z^2$ for all values of the parameters we tried. The number of PCG iterations required was 20–50 for $D = 1$ and 500–1000 for $D = \mathrm{d}^2/\mathrm{d}z^2$. In figure 7, we show the resulting reconstructed power densities. The reconstructions are quite accurate using surface data but using ring data we again observe spurious co-activation between brachialis and biceps.

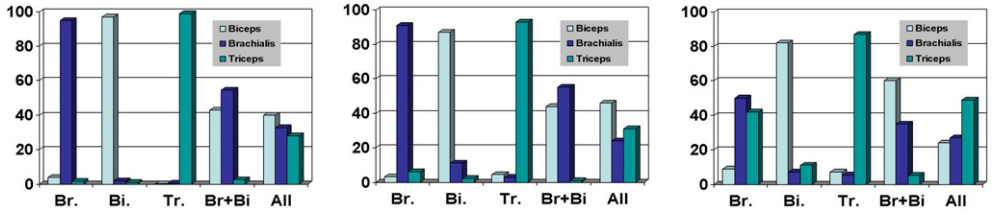

(a) Surface data, $D = 1$ (b) Surface data, $D = d^2/dz^2$ (c) Ring data, $D = 1$

Figure 7. Reconstructions of the power (total power normalized to 100) in biceps, brachialis and triceps. Artificial sources (with equal densities) were placed in the indicated muscles and reconstructions are shown for full data on the boundary and for data on the central ring. For the latter, no reasonable reconstruction using $D = \mathrm{d}^2/\mathrm{d}z^2$ could be obtained.

3.5. Experiment 4: bipolar human data

In this set of experiments we investigated the effect of using bipolar (differential) electrodes for sEMG measurement, with both human and synthetic data. The human sEMG data were obtained from a healthy human subject during isometric flexion and extension using a ring of 12 sensors around the upper arm. We used Delsys Bagnoli Desktop EMG Systems for the measurements. Differential sensors were employed since they are more widely used in sEMG than monopolar sensors, so it is important to determine if they can be used effectively with this method. However, theoretical arguments suggest that for our purposes monopolar sensors are much better suited. Differential sensors are popular as they reduce crosstalk from distant sources. The reason is that the spatial derivative of the EMG signal decays faster in the volume conductor than the monopolar signal [27]. However, this is the opposite of what we want for our application, as the information present in the crosstalk is used by our method to reconstruct the spatial information.

The sensors were placed approximately in the middle of the upper arm, aligned with the muscle fibers, in the configuration depicted in figure 2. The subject's elbow was placed at a flexion angle of about 90°, with the wrist supinated. In exercise I, the subject applied an isometric force by flexing the elbow. This is expected to activate the biceps and brachialis but not the triceps. Data were taken at 1000Hz for 15 s. In exercise II, the subject performed an isometric extension and data were taken in the same fashion. This is expected to mainly activate the triceps but possibly also the other two muscles which provide stabilization.

As we currently have no MRI data of our subject, we used the generic arm muscle model from [15], scaled to match the measured circumference (30cm) of the subject's arm at the location of the electrodes. For this sensor configuration, i.e. bipolar sensors in a ring, we found using tests with synthetic data that $\boldsymbol{D} = \mathrm{d}^2/\mathrm{d}z^2$ (i.e. reconstructing V rather than I directly) performed significantly better than $\boldsymbol{D} = 1$. The number of PCG iterations required was also much smaller than with the monopolar array, about 20–50.

Best results were obtained, upon a rough parameter trial and error, upon using $\mu_r = \beta$ in the ROI, $\beta = 0.1$, and a properly normalized anisotropic smoothing matrix $\boldsymbol{W} = \mathrm{diag}(1, 1, 10^{-3})$. A random sample of the middle 1 s of the data was chosen for the reconstruction. No significant difference was observed by the choice of sample. Besides the human data, we also generated corresponding synthetic data with 5000 sources distributed over biceps and brachialis for the first exercise and with 5000 sources in the triceps only for the second exercise. The reconstruction results are depicted in figures 8 and 9, respectively.

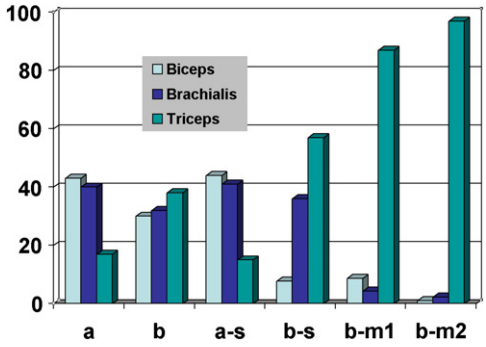

Figure 8. Relative current source power densities in three muscles, total power normalized to 100. Reconstructions were performed using human sEMG data during flexion (a) and extension (b). A generic morphometric model of the arm was used, scaled to match the circumference of the subjects arm. The results (a) look plausible as the main activity is in the biceps and brachialis. The result (b) from isometric extension of the triceps suggests a significant amount of co-activation of the biceps and brachialis, which is also plausible, as it is difficult not to activate these muscles for stabilization during the exercise. To check for consistency, we generated synthetic data and corresponding reconstructions by placing 5000 simulated tripole sources in biceps and brachialis (a-s) and then just in the triceps (b-s). The synthetic result (a-s) is very close to the real result (a), but the synthetic results (b-s) which should only show activity in the triceps show a significant amount of spurious co-activation in the brachialis, though not as much as in the real result (b). This is an indicator that the sensor configuration is inadequate to distinguish individual muscles accurately. To verify this hypothesis, we computed synthetic data for a ring of 56 monopolar (b-m1) and for a surface grid of 215 monopolar sensors (b-m2): it can be seen that the erroneous co-activation of the brachialis is no longer present.

The results were again visualized using COMSOL tools, and we depict illustrative isosurfaces chosen such that the two most active muscles are shown.

Note that the data are matched very well with the reconstructed sources. To quantify relative activation of muscles, we again display the relative power density. The results of the human data and synthetic data reconstructions are very similar for exercise I and are consistent with what one would expect. For exercise II, we observe in the human data reconstruction activity not just in the triceps but also in the other two muscles. It is quite plausible that biceps and brachialis are also activated for stabilization; however, this conclusion cannot be drawn from our results, for the reconstruction with synthetic sources *only* in the triceps also indicates spurious activation of the brachialis, though less so for the biceps. This clearly indicates the inadequacy of bipolar sensors (at least in this configuration); indeed if we reconstruct the same source model (5000 sources in the triceps only) using simulated monopolar data, then the desirable reconstruction is obtained, namely activity in the triceps only.

In summary we see that in this configuration, while the activities of individual muscles can still be discriminated to some extent, significant 'bleeding' of reconstructed activity into nearby inactive muscles results in a low quality of the reconstruction. Experiments with synthetic data indicate that monopolar sensors will greatly improve the quality of the reconstruction, which is also to be expected on theoretical grounds.

Another important observation is that the results from synthetic and human data are consistent, so we are confident that conclusions drawn from experiments with synthetic data are reliable and carry over to human data.

Although the 3D arm model used for the analysis of human data was just a generic model based on an anatomy book [15], the inversion has produced reasonably good results. To more

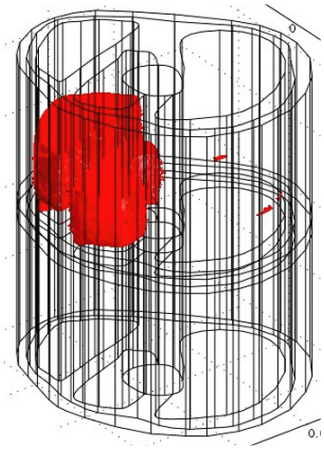

(a) Real data: isometric exion

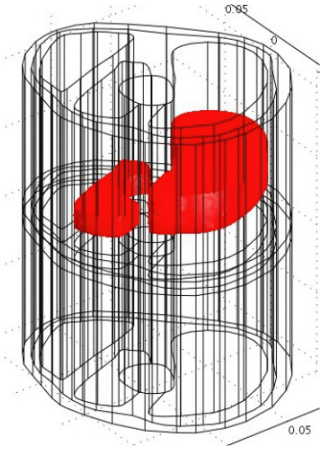

(b) Real data: isometric extension

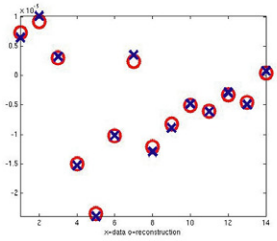

(c) x = data, o = reconstruction

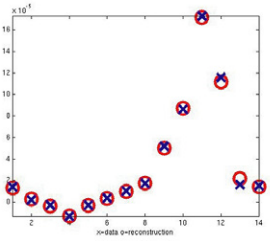

(d)

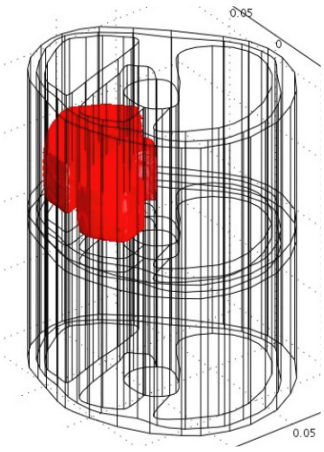

(e) Synthetic data: biceps and brachialis active

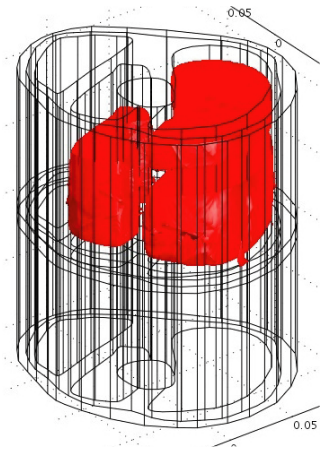

(f) Synthetic data: triceps only

Figure 9. Activity reconstructions using human data (a), (b) and synthetic data (e), (f). Illustrative isosurfaces of the reconstructed source fields and the match between input data and reconstructed data are depicted (c), (d), (g), (h). The bars labeled a, b, a-s, b-s in figure 8 correspond to (a), (b), (e), (f) in the current figure, respectively.

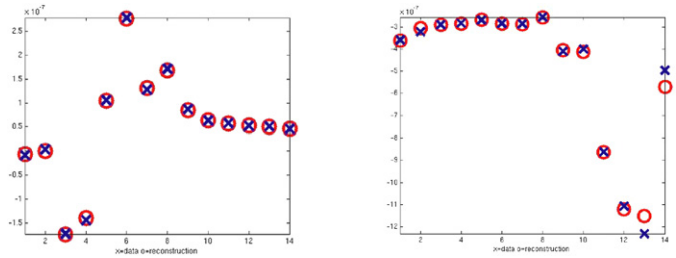

(g) (h)

Figure 9. (Continued.)

properly evaluate the effect of the anatomy on the reconstruction, we plan to acquire MRI data in the future.

Regarding the performance of our PCG solver, for $\boldsymbol{D} = \mathbf{1}$ the number of iterations is typically an agreeable 20–50. But for $\boldsymbol{D} = \mathrm{d}^2/\mathrm{d}z^2$, convergence can be very slow. We found that in experiment 4 the number of iterations was again 20–50, but up to 1000 iterations were required in experiments 2 and 3. A more sophisticated preconditioner is then required to speed up the computation, especially if computational efficiency is of prime importance. However, there is no practical need for this in the experimental setups we have considered as the only case where $\boldsymbol{D} = \mathrm{d}^2/\mathrm{d}z^2$ clearly outperforms $\boldsymbol{D} = \mathbf{1}$ is experiment 4, and for that particular configuration of sensors the PCG solver again converges quite fast.

We have also verified, by solving (5) directly[2], that the poor reconstructions in those cases where convergence is slow are not an artifact of the iterative solver.

4. Conclusions

We have described a new CMG technique that utilizes an underdetermined distributed source model to solve an important problem in muscle function monitoring. Results from simulated experiments with synthetic data indicate that a surface grid of monopolar sEMG sensors, similar to configurations used in EEG, is to be preferred over the more commonly used bi- or tripolar voltage sensors. The results obtained with human data using bipolar sensors are consistent with the results obtained from simulated data, even though the 3D arm model used for the analysis of human data was just a generic model. This suggests that simulated experiments are reliable indicators for the performance of the CMG system.

With our method, there is a choice between reconstructing the transmembrane current density ($D = 1$) and the intracellular action potential ($D = \mathrm{d}^2/\mathrm{d}z^2$). It was found that for monopolar surface data, $D = 1$ gives slightly better reconstructions than $D = \mathrm{d}^2/\mathrm{d}z^2$; the corresponding computation is also faster by at least an order of magnitude. For single source localization, $D = \mathrm{d}^2/\mathrm{d}z^2$ was able to correctly localize a deep source where $D = 1$ failed. For other source locations, there was no difference. In the experiment with monopolar ring data $D = \mathrm{d}^2/\mathrm{d}z^2$ failed to give good results, whereas in the experiment with bipolar ring data the situation was reversed. We currently have no theoretical explanation for this behavior.

All reconstructions were performed on a desktop computer with a dual core 3 GHz processor and 4 GB of RAM. Processing of sEMG data to produce the source estimations typically lasted 15 min, except for the case $D = \mathrm{d}^2/\mathrm{d}z^2$ with monopolar data where the

[2] This direct computation required about 24 h of computation time and 60 GB of RAM.

employed preconditioner for the PCG solver performed poorly requiring several processing hours. Fortunately, this does not pose a practical problem as the formulation with $D = 1$ produced superior reconstructions.

In the immediate future, we plan to test the CMG system with human data from monopolar sensors. We will also acquire a more complete and patient-specific 3D upper arm model from a set of cross-sectional MR images at different elevations. (To recall, the model used for our present results is based on an image of a single slice and is symmetric in the vertical axis.) Other issues include the experimental determination of the number of sEMG sensors required for good practical reconstructions and the sensitivity to location errors in the electrode placement. EMG systems with 64 or more channels are readily available, but it is not clear how many sensors can be fitted on the upper arm while still making good contact with the skin.

To validate the results obtained from human data, an independent measure of muscle activations is necessary to compare with the CMG predictions. Since we need the activations in the bulk of the muscles, verification with multiple single unit needle EMG recordings would be highly intrusive. Instead, we plan to use MRI to monitor exercise-induced signal changes which are primarily due to an increase or decrease in the transverse relaxation time of tissue water [12, 21].

References

[1] Bizzi E, Cheung V C, d'Avella A, Saltiel P and Tresch M 2008 Combining modules for movement *Brain Res. Rev.* **57** 125–33

[2] Chauvet E, Fokapu O and Gamet D 2001 Inverse problem in the surface EMG: a feasibility study *Proc. 23rd Annual EMBS Int. Conf. (Istanbul, Turkey)* pp 1048–50

[3] Curt A, Schwab M E and Dietz V 2004 Providing the clinical basis for new interventional therapies: refined diagnosis and assessment of recovery after spinal cord injury *Spinal Cord* **42** 1–6

[4] de Luca C J, Adam A, Gilmore L D and Nawab S H 2006 Decomposition of surface EMG signals *J. Neurophysiol.* **96** 1646–57

[5] Dietz V and Curt A 2002 Neurological aspects of spinal-cord repair: promises and challenges *Lancet Neurol.* **5** 688–94

[6] Dobkin B H, Curt A and Guest J 2006 Cellular transplants in China: observational study from the largest human experiment in chronic spinal cord injury *Neurorehabil. Neural Repair* **5** 5–13

[7] van den Doel K and Ascher U 2006 On level set regularization for highly ill-posed distributed parameter estimation problems *J. Comp. Phys.* **216** 707–23

[8] van den Doel K and Ascher U 2007 Dynamic level set regularization for large distributed parameter estimation problems *Inverse Problems* **23** 1271–88

[9] Drost G, Stegeman D F, van Engelen B G M and Zwarts M J 2006 Clinical applications of high-density surface EMG: a systematic review *J. Electromyogr. Kinesiol.* **16** 586–602

[10] Ellaway P H *et al* 2004 Towards improved clinical and physiological assessments of recovery in spinal cord injury: a clinical initiative *Spinal Cord* **42** 325–37

[11] Fuchs M, Wischmann H A and Wagner M 1994 Generalized minimum norm least squares reconstruction algorithms *ISBET Newslett.* **5** 8–1

[12] Giodano S B and Segal R L 2006 Leg muscles differ in spatial activation patterns with differing levels of voluntary plantarflexion activity in humans *Cell Tissues Organs* **184** 42–51

[13] Gorodnitzki I F, George J S and Rao B D 1995 Neuromagnetic source imaging with FOCUSS: a recursive weighted minimum norm algorithm *Electroencphalogr. Clin. Neurophysiol.* **95** 231–51

[14] Grave de Peralta Menendez R and Andino S L Gonzalez 1998 A critical analysis of linear inverse solutions *IEEE Trans. Biomed. Eng.* **45** 440–8

[15] Gray H 1858 *Henry Gray's Anatomy of the Human Body* (Yahoo online edition)

[16] Greenblatt R E 1993 Probabilistic reconstruction of multiple sources in the neuroelectromagnetic inverse problem *Inverse problems* **9** 271–84

[17] Hämäläinen M S and Ilmoniemi R J 1994 Interpreting magnetic fields of the brain-minimum norm estimates *Med. Biol. Eng. Comput.* **32** 35–42

[18] Helmholtz H L F 1853 Ueber einige gesetze der verheilung elektrischer ströme in körperlicher leitern mit anwendung auf die thierisch-elektrischen versuche *Ann. Phys. Chem.* **9** 211–33
[19] Jesinger R A and Stonick V L 1994 Processing signals from surface electrode arrays for noninvasive 3D mapping of muscle activity *IEEE DSP Workshop Proc.* pp 57–60
[20] Kilner J M, Baker S N and Lemon R N 2002 A novel algorithm to remove electrical cross-talk between surface EMG recordings and its applicaiton to the measurement of short term synchronization in humans *J. Physiol.* **538** 919–30
[21] Kinugasa R, Kawakami Y and Fukunaga T 2006 Quantitative assessment of skeletal muscle activation using muscle functional MRI *Magn. Reson. Imaging* **24** 639–44
[22] Lapatki B G, Jonas I E, Zwarts M J and Stegeman D F 2004 A thin, flexible multi-electrode grid for high-density surface EMG *J. Appl. Physiol.* **96** 327–36
[23] LoPresti E F, Jesinger R A and Stonick V L 1995 Identifying significant frequencies in surface EMG signals for localization of muscle activity *IEEE EMBS Conf. Proc.* pp 967–8
[24] Lowery M M, Stoykov N S, Taflove A and Kuiken T A 2002 A multiple-layer finite-element model of the surface EMG signal *IEEE Trans. Biomed. Eng.* **49** 446–54
[25] Marino R J, Ditunno J F Jr, Donovan W H and Maynard F (Jr) 2002 Neurologic recovery after traumatic spinal cord injury: data from the model spinal cord injury systems *Arch. Phys. Med. Rehabil.* **80** 1391–6
[26] McGill K C and Lateva Z C 2001 A model of the muscle-fiber intracellular action potential waveform, including the slow repolarization phase *IEEE Trans. Biomed. Eng.* **48** 1480–3
[27] Merletti R and Parker P A 2004 *Electromyography. Physiology, Engineering and Noninvasive Applications* (New York: IEEE)
[28] Michel C M, Murray M M, Lantz G, Gonzalez S, Spinelli L and de Peralta R G 2004 EEG source imaging *Clin. Neurophysiol.* **115** 2195–222
[29] Pascual-Marqui R D 2002 Standardized low resolution brain electromagnetic tomography (sLORETA): technical details *Methods Findings Exp. Clin. Pharmacol.* **24D** 5–12
[30] Rosenfalck P 1969 Intra- and extracellular potential fields of active nerve and muscle fibers: A physio-mathematical analysis of different methods *Acta Physiol. Scand.* **321 (suppl)** 1–168
[31] Stonick J T, Jesinger R A, Stonick V L and Baumann S B 1996 Estimation and localization of multiple dipole sources for noninvasive mapping of muscle activity *IEEE Int. Conf. Proc. on Acoustics, Speech, and Signal Processing, ICASSP-96* vol 5 pp 2912–5
[32] Vogel C 2002 *Computational Methods for Inverse Problem* (Philadelphia: SIAM)